Available on CMS information server **CMS CR PAS based on AN–2007/041, v1.1**

CMS Conference Report

26 December 2007

$\not\!\!E_T$ performance in CMS

CMS collaboration

Abstract

We present some aspects of missing transverse energy ($\not\!\!E_T$) reconstruction in CMS and provide performance benchmarks. $\not\!\!E_T$ corrections for jet energy scale, muons, and taus are discussed.

1 Introduction: $\not\!\!E_T$ in CMS

While a typical general-purpose collider detector has nearly 4π solid angle coverage, it is not completely hermetic, as it must have an opening in the very forward direction to feed the beams through it. Therefore, low p_T energetic interaction products, which move in very forward direction can escape detection, thus making it impossible to utilize total energy balance in the collision as a useful constraint. However, although these escaping forward particles may carry significant longitudinal momentum (i.e., momentum in the direction along the beams), they nevertheless can not carry large transverse momentum due to the large pseudorapidity (η) coverage of a typical collider detector. In the case of the CMS detector [1], this coverage ranges from -5 to $+5$.

Consequently, the detector allows for rather precise tests of the 2D-momentum conservation in the plane perpendicular to the direction of the beams. As a result, any significant imbalance in transverse momentum measured in the calorimeter is indicative of a production of a weakly interacting particle in the collision, which by itself indicates a process of interest. Among the standard model (SM) particles, such an imbalance would indicate the presence of either a muon or a neutrino. The momentum of the muon can be precisely measured combining the central tracker and the muon system, and the calorimeter-based missing transverse momentum can be corrected for its presence. The only SM particle that would truly escape the detection is a neutrino, and its presence could therefore be inferred from the remaining imbalance in total transverse momentum as measured by the calorimeter and the muon system.

Many extensions of the SM predict the existence of other weakly interacting stable or quasi-stable particles. Therefore, if an excess of events with significant transverse momentum imbalance is still observed after accounting for all the SM processes, it would constitute a strong evidence for new physics beyond the SM. This makes total transverse momentum imbalance (or *missing transverse momentum*) an important variable for searches for new physics.

Unfortunately, the flip-side of this coin is that the missing transverse momentum is extremely sensitive to various detector malfunctions and particles hitting poorly instrumented regions of the detector. Any dead or malfunctioning element in the detector may result in an artificial imbalance, thus mimicking the signal for new physics. Consequently, great care is required to understand the distribution in missing transverse momentum as measured by the detector and to ensure that it's a trustworthy variable for searches.

Historically, missing transverse momentum is often referred to as Missing Transverse Energy ($\not\!\!E_T$). This notation is somewhat confusing, as it commonly refers to either the 2D-vector of missing transverse momentum, or to its magnitude. In this note we will use the following notations: $\not\!\!E_T$ is the scalar variable, which describes the magnitude of the missing transverse momentum vector, while $\vec{\not\!\!E}_T$ refers to the 2D-vector itself. We will also use $\not\!\!E_x$, $\not\!\!E_y$ to denote the two components of the $\not\!\!E_T$ 2D-vector. In some cases, when the two projections correspond to a specially chosen axis and the directions perpendicular to it, we will use $\not\!\!E_\parallel$, $\not\!\!E_\perp$ to denote the two projections. Finally, we will use $\phi(\not\!\!E_T)$ to denote the azimuthal direction of $\vec{\not\!\!E}_T$.

$\vec{\not\!\!E}_T$ is an important variable for electroweak measurements and for searches for new physics with CMS. The $\not\!\!E_T$ values in processes of interest in CMS range from "small," e.g. in Higgs decays or Standard Model processes such as top and W production, to "large" in the decays of SUSY particles or due to escaping gravitons in scenarios with large extra dimensions. In the former case a good understanding of the QCD and environmental backgrounds is needed, as well as a good low-energy resolution. For large $\not\!\!E_T$ values the understanding of the tails is the main experimental challenge.

In this Physics Analysis Summary we describe the present state of the $\not\!\!E_T$ algorithms and studies. A discussion of the $\not\!\!E_T$ reconstruction is presented, as well as its performance. The primordial $\not\!\!E_T$ is calculated from energy deposits in the CMS Calorimeter Towers (CaloTowers), but to improve its central value and resolution several corrections have been studied, notably those due to jet energy scale, and due to the presence of muons and taus in the event. Finally we conclude with a number of points for future studies.

2 $\not\!\!E_T$ Reconstruction

The Missing Transverse Energy ($\not\!\!E_T$) is determined in the recent versions of the CMS software framework, CMSSW, from the transverse vector sum over uncorrected energy deposits in projective Calorimeter Towers:

$$\vec{\not\!\!E}_T = -\sum_n (E_n \sin\theta_n \cos\phi_n \hat{\mathbf{i}} + E_n \sin\theta_n \sin\phi_n \hat{\mathbf{j}}) = \not\!\!E_x \hat{\mathbf{i}} + \not\!\!E_y \hat{\mathbf{j}} \quad (1)$$

where the index n runs over all calorimeter input objects (e.g. energy deposits in towers, reconstructed hits, or generator-level particle energies). Here $\hat{\mathbf{i}}$, $\hat{\mathbf{j}}$ are the unit vectors in the direction of the x and y axis of the CMS right-handed coordinate system, where z is pointing in the direction of the beam, and x is horizontal. Note that in the absence of $\not\!\!E_T$ from physics sources in the event, $\not\!\!E_x$ and $\not\!\!E_y$ are expected to be distributed as Gaussians with a mean of zero and a standard deviation of σ, while $\not\!\!E_T$ has a more complicated shape described by $\frac{\sqrt{2\pi}}{\sigma}\theta(\not\!\!E_T)\not\!\!E_T \times G(\not\!\!E_T, 0, \sigma)$, where $\theta(x)$ is the θ function (i.e., 1 for $x \geq 0$ and 0 otherwise), $G(x, \mu, \sigma) = \exp(-(x-\mu)^2/2\sigma^2)/\sqrt{2\pi}\sigma$ is a Gaussian with the mean μ and standard deviation σ. Note that σ in the Gaussian describing $\not\!\!E_T$ is the same as the standard deviation in the $\not\!\!E_T$ projection onto an arbitrary axis. It is further trivial to show that:

$$\langle \not\!\!E_T \rangle = \sigma\sqrt{\frac{\pi}{2}} \approx 1.253\sigma; \tag{2}$$

$$\sigma(\not\!\!E_T) = \sigma\sqrt{\frac{4-\pi}{2}} \approx 0.655\sigma, \tag{3}$$

where $\sigma(\not\!\!E_T)$ is the r.m.s. of the $\not\!\!E_T$ distribution.

The Scalar Transverse Energy (ΣE_T), or total visible E_T in the event is defined as the scalar sum:

$$\Sigma E_T = \sum_n E_n \sin\theta_n,$$

where the index n runs over the same input objects as for $\not\!\!E_T$. In the barrel, energy in a single projective Calorimeter Tower is formed from the unweighted sum over energy deposits in the 5×5 matrix of the EM Calorimeter (ECAL) crystals with that in a single Hadron Calorimeter (HCAL) tower. In the forward regions, a more complex association of ECAL crystals with HCAL towers is required.

$\not\!\!E_T$ is a global observable which depends on precise symmetric cancellations and hence is a good indicator of the health of the underlying input. The global nature of $\not\!\!E_T$ also means that disentangling and understanding the different factors affecting the performance can be very challenging. Most generally, the resolution of $\not\!\!E_T$ can be parameterised according to the following form:

$$\sigma(\not\!\!E_T) = A \oplus B\sqrt{\Sigma E_T - D} \oplus C\,(\Sigma E_T - D), \tag{4}$$

where the A ("noise") term represents effects due to electronic noise, pile-up (PU), and underlying event (UE); the B ("stochastic") term represents the statistical sampling nature of the energy deposits in individual Calorimeter Towers; the C ("constant") term represents residual systematic effects due to non-linearities, cracks, and dead material; and D ("offset") represents the effects of noise and pile-up on $\sum E_T$. It is important to emphasize that the above parameterization factorizes A, B, C into *a priori* uncorrelated effects. In particular, the stochastic and constant terms do not depend, to first order, on the effects of noise, pile-up, or underlying event. Hence, the offset due to noise must be explicitly taken into account when comparing the $\not\!\!E_T$ performance between samples having different noise thresholds and pile-up conditions – this can often be a dramatic effect, if not properly addressed.

3 $\not\!\!E_T$ Performance in CMSSW_1_5_2

The data samples used to study the $\not\!\!E_T$ performance were produced with recent versions of the CMS Software Framework, CMSSW. The Monte Carlo generation and particle propagation step was performed using version CMSSW_1_4_x, while the digitization and reconstruction step was performed with CMSSW_1_5_2. The samples correspond to QCD dijets produced in eleven bins of $\hat{p}_T$ between 20 GeV and not more than 800 GeV and contained no pile-up. Here $\hat{p}_T$ is the transverse momentum of the particles in the center-of-mass frame of the $2 \rightarrow 2$ parton scattering. At leading order, it is close to the transverse momentum of the jets produced in the scattering in either the center-of-mass or detector frame.

Figure 1 illustrates the $\sigma(\not\!\!E_x)$ and $\langle \not\!\!E_T \rangle$ vs. ΣE_T for QCD dijet samples with $20 < \hat{p}_T < 800$ GeV. To facilitate comparison of the stochastic and constant terms in these fits to those obtained in previous studies (which include different thresholds and events with pile-up), an offset, $\langle \Sigma E_T \rangle_{\texttt{min}}$, is explicitly included as a variable parameter in the fit. The fit to the full range of data points yields the following functions:

$$\begin{aligned}
\sigma^2(\not\!\!E_x) &= (1.53\ \text{GeV})^2 + (104\%\ \text{GeV}^{1/2})^2(\Sigma E_T - 77\ \text{GeV}) + (2.55\% \times (\Sigma E_T - 77\ \text{GeV}))^2; \\
\sigma^2(\not\!\!E_T) &= (1.48\ \text{GeV})^2 + (103\%\ \text{GeV}^{1/2})^2(\Sigma E_T - 82\ \text{GeV}) + (2.32\% \times (\Sigma E_T - 82\ \text{GeV}))^2.
\end{aligned}$$

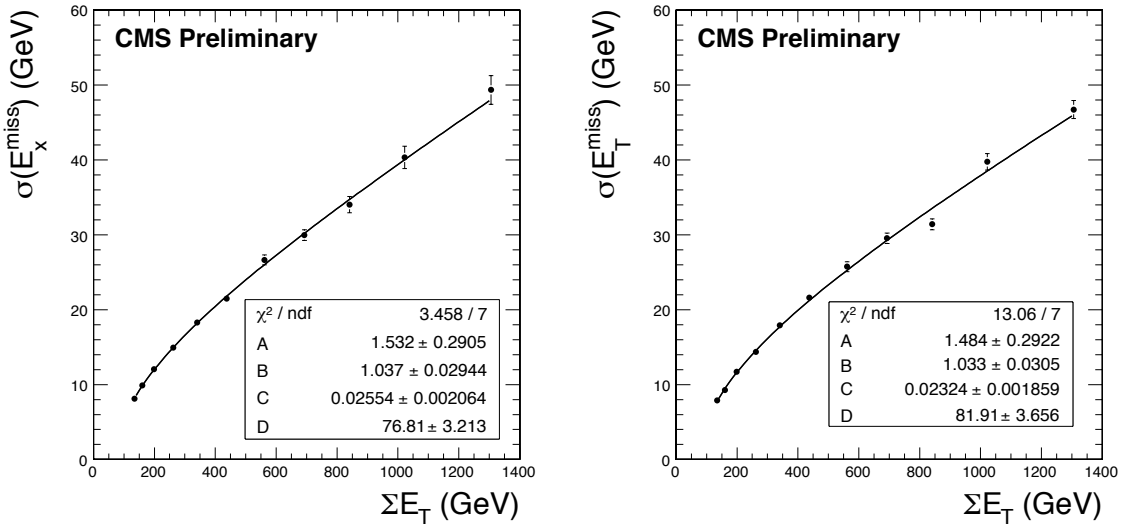

Figure 1: $\sigma(\not\!\!E_x)$ (left) and $\sigma(met)$ (right) vs. ΣE_T for QCD dijet samples without pile-up for $20 < \hat{p}_T < 800$ GeV (black dots). The resolution fit is shown by the black line. The fit parameters correspond to the corresponding terms in Eq. (4).

The first terms correspond to the effects of electronic noise in an "empty" (or collision-less) event. Due to such noise, "empty" events will have a minimum average visible total transverse energy, $\langle \Sigma E_T \rangle_{\mathtt{min}}$, which is seen to be around 80 GeV. It is important to note that because the dataset conditions are very different in this study with respect to the PTDR [2] (the datasets studied in this work have different calorimeter cell thresholds and no pile-up, for example), the A term can not be easily compared with the earlier PTDR results. The second, B, term represents the stochastic effects of a sampling calorimeter and can be more easily compared with the earlier results of the PTDR: in the case of the PTDR, $\sigma(\not\!\!E_x)$ had a stochastic term of 97% [2]. The third (C or constant) term can also be compared with the earlier results of the PTDR: in the case of the PTDR, $\sigma(\not\!\!E_x)$ had a constant term of 1.2%. The stochastic and constant terms are higher with respect to the PTDR because the simulation of the calorimeters has been significantly improved to yield more realistic detector performance.

4 $\not\!\!E_T$ Corrections

4.1 Introduction

The Calorimeter Tower based $\not\!\!E_T$ calculation can be improved by correcting $\not\!\!E_T$ for several effects. First there are the Jet Energy Scale corrections, also often called Type I corrections. These corrections take the measured raw energy values and adjust them for the difference between the raw jet energy and the true jet energy, as defined by the Jet Energy Scale (JES) group [3].

Events may also contain muons. In the majority of cases the muon deposits only very little energy in the calorimeters. Hence to correct for the muon response the actual muon momentum measurement from the central tracker and muon system is used to replace the energy measured along the muon trajectory in the calorimeter.

Isolated taus yield jets that differ substantially from average QCD jets. Specific corrections for τ-jets based on particle flow methods can be employed in this case.

Besides the corrections to the high p_T objects as listed above, there are effects due to the soft underlying event, pile-up etc. These so called Type II corrections have not been studied within the CMSSW framework as of yet. Developing these corrections is one of the high-priority future tasks for the JetMET group.

The $\not\!\!E_T$ corrections aim to bring the measured $\not\!\!E_T$ value closer to the true $\not\!\!E_T$ on event by event basis, and to improve the resolution of the $\not\!\!E_T$ variable in general. The individual corrections are described in this section.

4.2 Type I Jet Energy Scale Corrections

Type I corrections to $\not\!\!E_T$ are based on the energy response of jets reconstructed in the event. They are essential to remove biases in the determination of $\not\!\!E_T$ due to the non-linear response of the calorimeter to jet energy deposits at different values of E_T and rapidity. We first define JES corrections and then discuss how they affect the $\not\!\!E_T$ bias and resolution.

Reliable MC jet corrections are the first step toward realistic jet corrections based on data. They allow to test various methods and develop techniques to quickly derive the corrections with data. Standard MC-based jet (MCJet) corrections [4] resolve jets as a function of two variables: transverse energy (E_T^j) and pseudorapidity ($|\eta_j|$). The MCJet-corrections are derived by fitting the relative response of the calorimeter, defined as the ratio of transverse energies of the reconstructed and MC-generated jets, E_T^j(Rec)/E_T^j(MC), with a Gaussian in each E_T^j, $|\eta_j|$ bin. This technique takes into account non-uniformity and nonlinearity of the calorimeter [4].

The CMS calorimeter system is non-compensating, i.e. its response to neutral and charged pions is very different. This effect can be taken into account by adding the third variable in the derivation of jet corrections: the fraction of jet energy deposited in the ECAL (EM fraction, or EMF) [5]. These three variables contain most of the information about a jet. They are derived based on the absolute response of the calorimeter, E_T^j(Rec)$-E_T^j$(MC), which is more Gaussian than the relative response, especially at low jet E_T. The current scheme of JES corrections in CMS, calls for factorization of various corrections. The EMF-based correction is applied on top of the MCJet one [3] and in what follows, we refer to it as MCJet+EMF correction. It has been demonstrated [5] that accounting for the jet EMF does improve jet energy resolution by about 10% compared to the result of just the MCJet corrections.

When applying the Type I corrections, care has to be taken to avoid applying the jet response corrections to electrons reconstructed as jets with high fraction of EM energy; such jets can be identified, e.g., by matching to reconstructed electrons. In addition, average MCJet corrections are also not applicable to true jets with high EM fraction; furthermore the MCJet+EMF-corrections for such jets are already small. Type I corrections are therefore not applied for jets which exceed a certain EMF threshold. Jets with p_T^j lower than 10 GeV are excluded as well, as the jet energy corrections for these are known to have large uncertainties.

A standard CMSSW package corrects jets according to one of the official algorithms used for JES corrections (the default is MCJet). $\not\!\!E_T$ is corrected according to the following formula:

$$\vec{\not\!\!E}_T^{\,\mathrm{corr}} = \vec{\not\!\!E}_T - \sum_{i=1}^{\mathrm{N_{jets}}} \left[\vec{p}_{T_i}^{\,\mathrm{corr}} - \vec{p}_{T_i}^{\,\mathrm{raw}}\right],$$

where the sum runs over all the jets not identified as electrons or photons, which have p_T^{raw} greater than the chosen threshold.

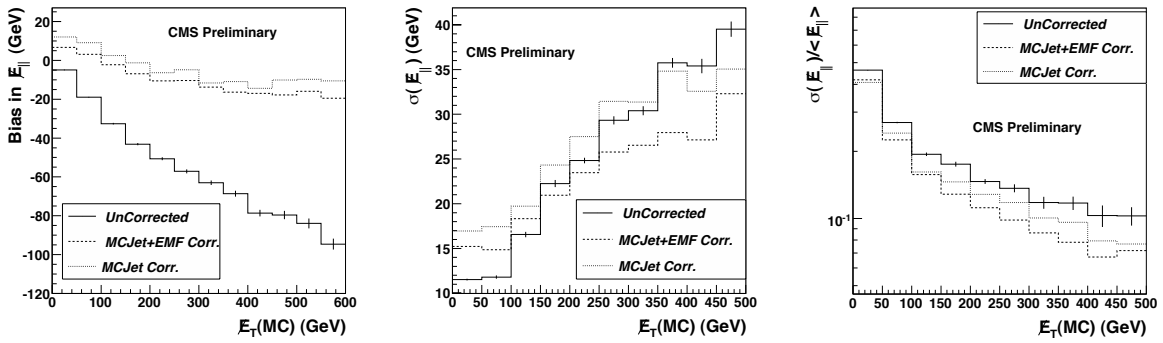

Figure 2: $\not\!\!E_{\parallel}$ bias and resolution in the $W(e\nu)+$ jets sample. Left: $\not\!\!E_{\parallel}$ bias as a function of $\not\!\!E_T$(MC). Center: absolute resolution, $\sigma(\not\!\!E_{\parallel})$, as a function of $\not\!\!E_T$(MC). Right: relative resolution, $\sigma(\not\!\!E_{\parallel})/\not\!\!E_{\parallel}$, as a function of $\not\!\!E_T$(MC).

We applied both MCJet and MCJet+EMF JES corrections to events with true $\not\!\!E_T$ using $W(e\nu)+$ jets samples produced in CMSSW_1_3_X. This sample allows to see the effect of the corrections as a function of either $\sum E_T$ or $\not\!\!E_T$ in a large range.

In order to demonstrate the effect of Type I $\not\!\!E_T$ corrections, we define the parallel component of $\not\!\!E_T$ ($\not\!\!E_{\parallel}$), which

is the projection of the reconstructed $\not\!\!E_T$ on the direction of the neutrino produced in the W decay, as determined at the generator level (p_ν). This direction is the direction of "true" $\not\!\!E_T$ in the event, and thus allows to study both the bias and resolution in the presence of true $\not\!\!E_T$.

Most importantly, both MCJet and MCJet+EMF corrections nearly remove significant bias in $\not\!\!E_\parallel$ vs. $\not\!\!E_T$(MC). This is particularly important at large $\not\!\!E_T$(MC) (see the left plot in Fig. 2). Both the absolute and relative $\not\!\!E_\parallel$ resolutions, defined as $\sigma(\not\!\!E_\parallel)$ and $\sigma(\not\!\!E_\parallel)/\not\!\!E_\parallel$), as a function of the true $\not\!\!E_T$ in the event, $\not\!\!E_T$(MC), are shown in Fig. 2. Significant improvement is achieved in relative $\not\!\!E_\parallel$ resolution, primarily due to removed $\not\!\!E_T$ bias, which increases overall $\not\!\!E_\parallel$ found in the denominator of the expression for relative resolution. One can also see from this figure that MCJet+EMF corrections work substantially better than MCJet only corrections. The reason absolute resolution is not reduced significantly after applying JES corrections is that the latter increase the overall transverse energy in the event, which in turn worsens $\not\!\!E_T$ resolution, as indicated by Eq. (4).

4.3 Muon corrections

Missing transverse energy has to be also corrected for the muon objects in the event. As a muon is a minimum ionizing particle over the wide range of a particle momentum, it deposits only a small amount of energy in the calorimeter, typically a few GeV, and thus can create a fake $\not\!\!E_T$. Therefore, the transverse momenta of all muons in the event are subtracted vectorially from the $\not\!\!E_T$ vector, after deduction of the energy deposition of the muons in the calorimeter:

$$\vec{\not\!\!E}_T = -\sum_{i=1}^{\text{towers}} \vec{E}_T^{\,i} - \sum^{\text{muons}} \vec{p}_T^{\,\mu} + \sum_{i=1}^{\substack{\text{deposit}\\ \text{towers}}} \vec{E}_T^{\,i}.$$

The $\not\!\!E_T$ muon corrections are studied using using $Z \to \mu^+\mu^-$ Monte Carlo (MC) samples reconstructed with CMSSW_1_3_1. Here we focus on the "high p_T" sample with $230 < p_T^Z < 300$ GeV.

Muons are identified combining information from the inner tracker and the muon system. The analysis starts with the muons separated from jets by at least 0.5 in the η–ϕ space, with $p_T^\mu > 10$ GeV and $|\eta^\mu| < 2.4$ and passing certain quality cuts. We calculate the direction of the Z boson by selecting events with two good muons, and divide $\not\!\!E_T$ into two components: parallel ($\not\!\!E_\parallel$) and perpendicular ($\not\!\!E_\perp$) to the Z direction. The "raw" $\not\!\!E_T$ tends to lie along the Z direction, as the dominant $\not\!\!E_T$ source is muon energy which is not registered in the calorimeter. The estimated $\not\!\!E_T$ resolution in the orthogonal direction $\not\!\!E_\perp$ is dominated by the underlying event and pile-up activity and nominally Gaussian distributed around zero. Figure 3 shows the $\not\!\!E_\parallel$ distribution of $Z \to \mu\mu$ events. The "raw" $\not\!\!E_\parallel$ distributions (thin solid line) are shifted towards positive values, especially for large values p_T of the Z boson.

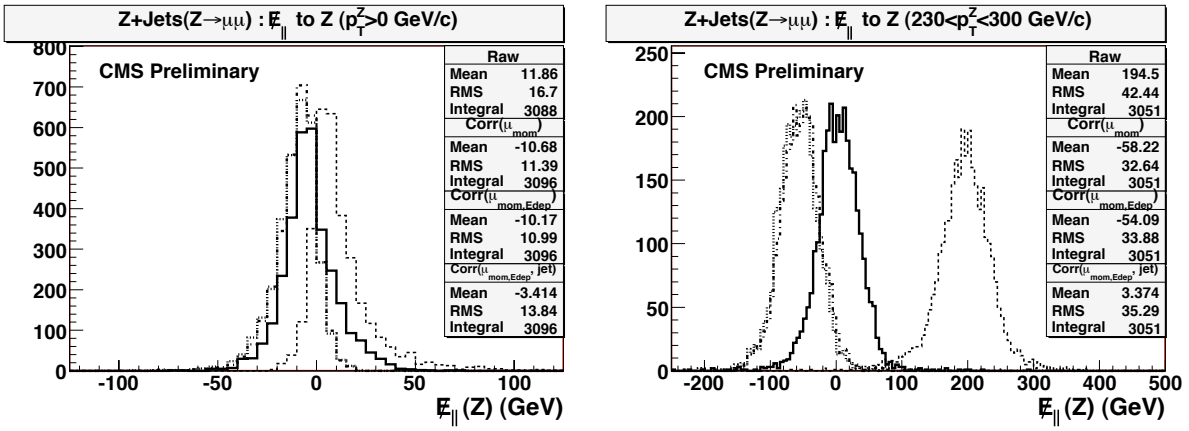

Figure 3: Distributions of $\not\!\!E_\parallel$ ($\not\!\!E_T$ component parallel to the reconstructed Z direction) in the inclusive (left) and high p_T (right) $Z \to \mu\mu$ samples. The histograms represent $\not\!\!E_\parallel$ distributions at different correction levels: uncorrected "raw" $\not\!\!E_\parallel$ (thin solid line), muon momentum correction (dotted line), muon momentum and muon energy deposit in the calorimeter (dash-dotted line), all muons and jet energy scale corrections (thick solid line).

The first step is to correct $\not\!\!E_T$ for the reconstructed muon energy. The 2-dimensional (p_x^μ, p_y^μ) muon momentum vectors are subtracted from the "raw" $\not\!\!E_T$ vector. Distributions of the $\not\!\!E_\parallel$ and $\not\!\!E_\perp$ after the muon momentum correction are shown in Fig. 3. The $\not\!\!E_\parallel$ distribution is shifted to negative values after the correction, which is

consistent with the presence of uncorrected jets back-to-back with the Z.

To avoid the double counting, it is necessary to take into account the muon energy deposited in the calorimeters. Projecting the tower energy onto the muon track direction, one obtains a 2D vector of the tower energy, which is then further propagated to the $\not\!\!E_T$ 2D vector. The dash-dotted distributions in Fig. 3 show the $\not\!\!E_{\parallel}$ distribution after taking the transverse muon energy deposited in the calorimeters into account. The impact of this correction is small, as expected.

The last step is the correction for the jet energy scale. This is performed as described in Section 4.2 (MCJet corrections). The results after applying this correction are shown in Fig. 3. After applying the JES correction, the $\not\!\!E_{\parallel}$ distribution is centered around zero, demonstrating that the jet energy correction successfully restores the average $\not\!\!E_T$ scale.

In the future, muon quality criteria for $\not\!\!E_T$ correction will be further exploited, as uncertainties in the behavior of badly reconstructed high p_T^{μ} muons may lead to the unphysical long tails in the $\not\!\!E_T$ distribution. The corrections due to the very low $p_T^{\mu} < 10$GeV muons are less important because their contribution to the $\not\!\!E_T$ resolution is smaller than the average measurement error based on the calorimeter response. Finally, preselection cuts are to be developed in order to reduce the "fake" $\not\!\!E_T$ due to the cosmic muons.

4.4 Tau corrections

Tau jets are substantially different from ordinary jets, making standard jet corrections inappropriate for taus. These differences arise from the fact that hadronic taus typically have a small number of fairly energetic particles while QCD jets of the same energy have higher multiplicity and a larger fraction of energy carried by soft particles. Applying standard jet corrections to hadronic tau jets results in a significant over-correction of $\not\!\!E_T$. The is illustrated in Fig. 4 which shows the distribution of $\not\!\!E_T^{\rm reco} - \not\!\!E_T^{\rm true}$ for visible hadronic tau energy in the $W \to \tau_{\rm had}\nu$ events for the cases without JES corrections (dashed line) and when standard MCJet corrections are applied (dash-dotted line). Neither case yields a satisfactory description of the jet p_T.

We define the $\not\!\!E_T$ correction procedure for hadronic tau jets, which satisfy certain identification requirements. To minimize biases, we use loose selection criteria to identify taus. The most powerful and discriminant against QCD jets is the narrow widths of the tau jet.

The $\not\!\!E_T$ correction is calculated as follows:

$$\Delta\vec{\not\!\!E}_T = \sum_{reg} \vec{E}_T^{\rm cal} - \vec{E}_T^{\tau} - \sum_{reg} \vec{E}_T^{\rm UE} - \sum_{\rm reg} \vec{E}_T^{\rm PU},$$

where the sum is over a region (reg) of the CaloTowers that fully contains the energy deposits of the tau decay products, typically corresponding to a cone of $\Delta R = 0.5$. The first term sums up energy deposition in the selected region of the calorimeter (with the same thresholds used in the calculation of raw $\not\!\!E_T$), and the second term is the true visible tau transverse energy. The third and fourth terms sum up true transverse energies of particles from underlying event and pile-up in the same calorimeter region. The latter is required to avoid the double counting of energy (energy depositions of these particles are counted towards raw $\not\!\!E_T$, but not in the tau energy). This formulation of the correction, however, implies that a correction for the underlying event (UE) and pile-up (PU) is applied everywhere in the detector, which is not typical for most analyses. Therefore, we modify the correction to include only residual UE and PU terms:

$$\Delta\vec{\not\!\!E}_T = \sum \vec{E}_T^{\rm cal} - \vec{E}_T^{\tau} - \vec{E}_T^{\rm UE\ res} - \vec{E}_T^{\rm PU\ res}, \tag{5}$$

Residual PU and UE energy is defined as energy measured in the calorimeter and (i) accounted for in the raw $\not\!\!E_T$ calculation, (ii) contributing to the first term, and (iii) not contributing to the second term.

The first term in Eq. (5) can be approximated by the transverse energy of a jet obtained using standard cone-based jet clustering algorithm with the cone size of 0.5 (modulo possible difference in energy thresholds used in calculating raw $\not\!\!E_T$ and in the jet energy summation). The second term should be approximated by the best available measurement of the tau energy, and is discussed below. The last two terms can be parameterized as a function of the number of primary vertices and measured in e.g. $Z \to ee$ events by looking in the direction away from the two leptons. However, these corrections will be small for early running conditions and are neglected here. Also, higher tower energy thresholds used in jet reconstruction further diminish the size of the residual correction due to UE and PU.

In selecting a specific technique to determine the tau energy, one has a choice between the particle flow (PF) measurement and the calorimeter measurement with tau specific corrections. The PF algorithm provides a very accurate measurement of the tau energy except at very high energies. However, the PF algorithm is not available at the trigger level, thus making it important to develop and understand corrections based on both algorithms. The calorimeter-based corrections were studied earlier and were found to improve the $\not\!\!E_T$ scale, but not the resolution [6]. Therefore, we will focus on the algorithm utilizing the PF-based tau energy measurement.

We define a minimal PF based $\not\!\!E_T$ correction for τ's as:

$$\Delta\vec{\not\!\!E}_T = \sum \vec{E}_T^{\text{cal jet } 0.5} - \vec{E}_T^{\text{PF } \tau},$$

To gauge the performance of this correction and disentangle effects associated with other corrections (e.g. for jets, electrons and muons), we select a sample of $W \rightarrow \tau\nu$ events and require that there be no additional jets with $E_T > 5$ GeV. While this is a harsh requirement, it is effective in removing other effects associated with mismeasurements of recoil jet energies. Figure 4 (right) shows the $(\not\!\!E_T{}^{\text{reco}} - \not\!\!E_T{}^{\text{true}})$ distribution for three cases: no correction (dashed line), standard jet correction (dash-dotted) and PF-based (solid) correction. The PF based calculation is seen to yield the result with the smallest bias and the best resolution. The absence of a visible bias confirms that effects of the UE are small. The residual efffects of the UE will nonetheless be studied and appropriate corrections will soon be available.

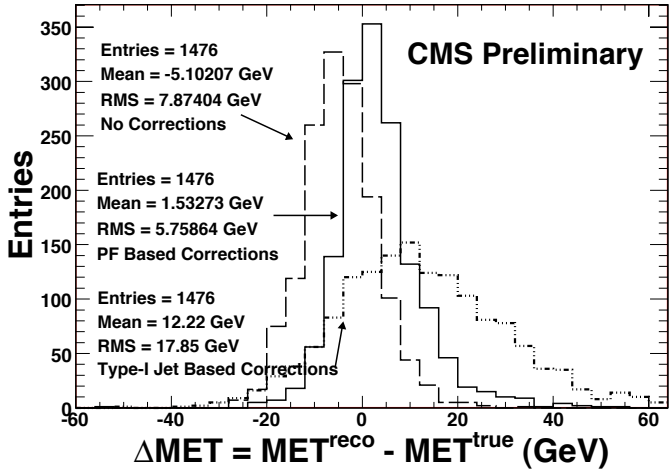

Figure 4: Distribution of $(\not\!\!E_T{}^{\text{reco}} - \not\!\!E_T{}^{\text{true}})$ for hadronically decaying tau leptons in $W(+0jets) \rightarrow \tau_{\text{had}}\nu$ events for three cases: no correction (dashed line), standard jet correction (dash-dotted), and PF-based (solid) correction.

We also would like to discuss the limits of applicability of the dedicated tau corrections. First, dedicated tau corrections improve the $\not\!\!E_T$ scale and resolution only in events that have real taus, and then only if these taus are identified as such. Applying these corrections to events where a QCD jet is misidentified as a tau will not lead to better $\not\!\!E_T$ resolution or scale. Therefore, in the vast majority of physics analyses that are not specifically targeting events with real taus, one should not use these corrections merely because a jet was tagged as a tau candidate. Second, even in analyses that target final states with hadronic taus, one will only improve $\not\!\!E_T$ in signal events and not in the backgrounds where a jet is misidentified as a hadronic tau. However, applying tau corrections to $\not\!\!E_T$ is appropriate in the second case as it improves separation between signal and backgrounds. It is also worth mentioning that applying standard jet corrections to jets misidentified as taus will generally not be correct either because tau-tagging procedures select rather peculiar jets, while standard jet corrections are derived from average jets.

Finally, the correction procedure we describe is defined only for hadronically decaying taus that satisfy certain identification requirements. If one uses a different identification procedure, these corrections may need to be recalculated. Fortunately, this will only become an issue if the tau tagging method is substantially different from what was used in obtaining these corrections.

5 Conclusions

This Physics Analysis Summary gives an account of the status of the missing transverse energy calculation and studies in CMS. Next are the study of the precision reach of data driven calibration and resolution estimate techniques versus luminosity. Future developments include:

- the study of pathological $\not\!\!E_T$ events in the Monte Carlo simulation of high-p_T QCD events;
- the study of different Type I corrections, more tailored to $\not\!\!E_T$ needs;
- the study of optimum muon and tau ID and kinematic cuts for the purpose of $\not\!\!E_T$ corrections;
- the development and study of Type II corrections for the soft underlying event contribution to $\not\!\!E_T$;
- the impact of pile-up on $\not\!\!E_T$ and the effect of mis-estimating $\not\!\!E_T$ due to the selection of the wrong primary vertex;
- The usage of (more) particle flow objects to improve the detector resolution and therefore the $\not\!\!E_T$ resolution;
- the study of the $\not\!\!E_T$ significance likelihood variable;
- the study of beam halo and cosmics background effects on $\not\!\!E_T$;
- the study of $\not\!\!E_T$ with real data during CMS cosmics runs in early 2008, followed by first real collider data in late 2008.

The $\not\!\!E_T$ variable is not an easy object to understand, so a long and dedicated study will be necessary to turn it into a useful physics analysis variable.

References

[1] For a Web page describing the CMS detector, see, e.g., `http://cms.cern.ch/iCMS`.

[2] CMS Collaboration *"CMS Physics Technical Design Report v.1: Detector Performance and Software,"* CERN LHCC/2006–001 (2006).

[3] S. Esen *et al.*, **CMS Analysis Note in Preparation**, *"Plans for Jet Energy Corrections at CMS."*

[4] M. Vazquez Acosta *et al.*, **CMS Note IN-2007/053**, *"Jet and MET Performance in CMSSW_1_2_0."*

[5] S. Esen and G. Landsberg, **CMS Internal Note in Preparation**, *"3D MCJet Corrections."*

[6] CMS Collaboration, *"Tau jet reconstruction and tagging with CMS"*, Eur. Phys. J C, **45**, Suppl. 1. Phys. Rev. D **13**, 3214 (1976).